ELECTRONIC SUPPLEMENTARY INFORMATION

Probing Lewis acidity of $Y(BH_4)_3$ via its reactions with MBH_4 (M = Li, Na, K, NMe_4)

Tomasz Jaroń [1,*] and Wojciech Grochala [1,2**]

[1] *Faculty of Chemistry, The University of Warsaw, Pasteura 1, 02093 Warsaw, Poland.*

[2] *ICM, The University of Warsaw, Pawińskiego 5a, 02106 Warsaw, Poland.*

** e-mail: tjaron@chem.uw.edu.pl, ** e-mail: wg22@cornell.edu*

Contents:

1. Figure S1. Rietveld plot of $KY(BH_4)_4$ refinement.
2. Figure S2. Rietveld plot of $(CH_3)_4NY(BH_4)_4$ refinement.
3. Table S3. Interatomic distances in $KY(BH_4)_4$ crystal.
4. Table S4. Interatomic distances in $(CH_3)_4NY(BH_4)_4$ crystal.
5. Table S5. Comparison of the ranges of bond lengths and angles in selected borohydrides.
6. Introduction to the FTIR spectra of $Y(BH_4)_3/MBH_4$ composites.
7. Figure S6. Infrared spectra of $Y(BH_4)_3 + MBH_4$ composites.
8. Table S7. Infrared absorption bands in the synthesised Y compounds compared with their Sc analogues.
9. Figure S8. Temperature-resolved FTIR spectrum of the gases evolved during the thermal decomposition process of $(CH_3)_4NY(BH_4)_4$.
10. Figure S9. MS of the gases evolved in the thermal decomposition of $(CH_3)_4NY(BH_4)_4$.
11. Figure S10. Temperature-resolved FTIR spectrum of the gases evolved during the thermal decomposition process of $(CH_3)_4NBH_4$.
12. Figure S11. MS of the gases evolved in the thermal decomposition of $(CH_3)_4NBH_4$.
13. Figure S12. PXD of the thermal decomposition products of $(CH_3)_4NY(BH_4)_4$.
14. Figure S13. Temperature-resolved FTIR spectrum of the gases evolved during the thermal decomposition of $KY(BH_4)_4$.
15. Figure S14. Temperature-resolved MS of the gases evolved in the thermal decomposition of K $Y(BH_4)_4$.
16. Figure S15. TGA and DSC profiles of KBH_4 milled for 1 h.
17. Figure S16. TGA and DSC profiles of $3KBH_4 + YCl_3$ milled for 1 h.

18. Figure S17. FTIR spectra of $KY(BH_4)_4$ thermal decomposition products at RT, (b) heated to 210 ^{O}C and cooled to RT, (c) heated to 295 ^{O}C and cooled to RT, (d) heated to 410 ^{O}C and cooled to RT, (e) KBH_4, (f) YH_x.

19. Figure S18. TGA and DSC profiles of KBH_4 milled for 1 h.

20. Figure S19. Rietveld plot of $Y(BH_4)_3$ + $NaBH_4$ + 3 LiCl composite measured at 171 ^{O}C.

21. Figure S20. Rietveld plot of $Y(BH_4)_3$ + $NaBH_4$ + 3 LiCl composite heated to 200 ^{O}C (5 K/min) and rapidly quenched (50 K/min); PXD measured at RT.

22. Figure S21. PXD pattern of $Y(BH_4)_3$ + $NaBH_4$ + 3 LiCl composite at 400 ^{O}C.

23. Figure S22. PXD pattern of $Y(BH_4)_3$ + $LiBH_4$ + 3 LiCl composite heated to 210 ^{O}C and quickly quenched to room temperature.

24. Figure S23. PXD pattern of $KY(BH_4)_3$ + 3 LiCl: (a) sample heated to 210 ^{O}C and quickly quenched to room temperature (black, top curve), measured for 17 h at room temperature; (b) measured at 200 ^{O}C for 5.5 h.

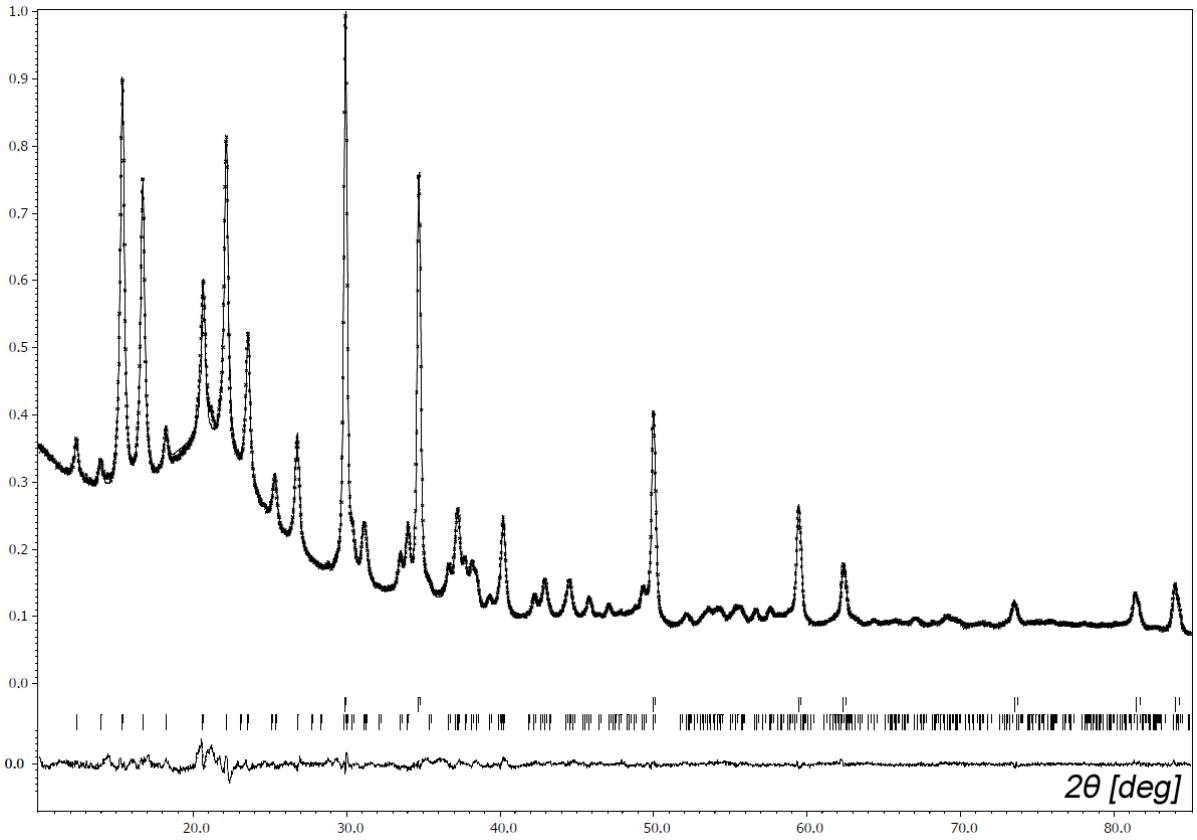

Figure S1. Rietveld plot from structure refinement of $KY(BH_4)_4$.

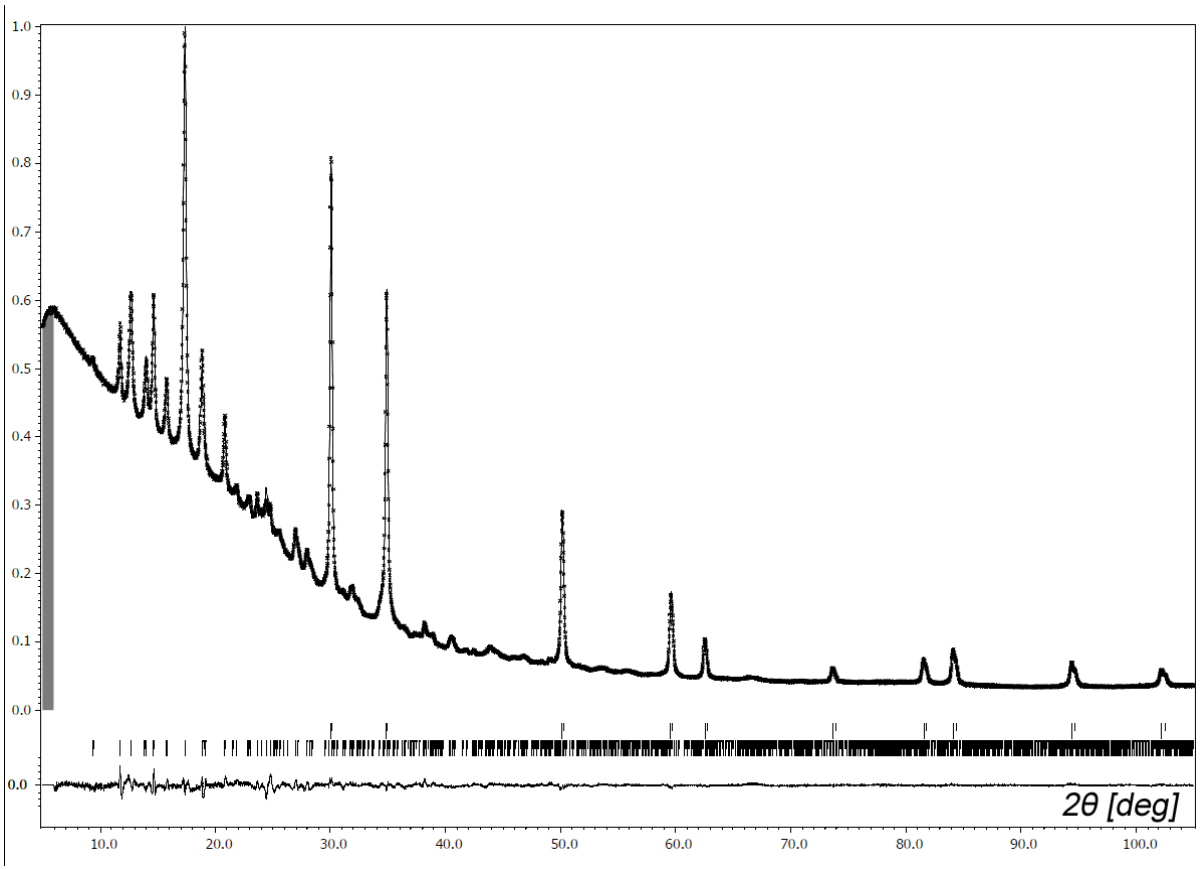

Figure S2. Rietveld plot from structure refinement of $(CH_3)_4NY(BH_4)_4$.

Table S3. Interatomic distances in $KY(BH_4)_4$ crystal.

$KY(BH_4)_4$	**PXD**
$(B - H)_{min}$	1.12(4)
$(B - H)_{max}$	1.12(4)
$(H - B - H)_{min}$	109(4)
$(H - B - H)_{max}$	109(4)
$(Y - H)_{min}$	2.20(3)
$(Y - H)_{max}$	2.41(4)
$(Y - H)_{averag.}$ x 12	**2.29**
$(Y - B)_{min}$	2.362(9)
$(Y - B)_{max}$	2.448(10)

$(Y - B)_{averag.}$ x 4	**2.405**
$(B - Y - B)_{min}$	108.44(16)
$(B - Y - B)_{max}$	112.3(4)
$(K - H)_{min}$	2.60(4)
$(K - H)_{averag.}$ x 6	**2.76**
$(K - H)_{max}$	3.37(3)
$(K - H)_{averag.}$ x 12	**3.34**
$(K - H)_{overall}$ x 18	**3.147**
$(K - B)_{min}$	3.259(10)
$(K - B)_{max}$	3.354(7)
$(K - B)_{averag.}$ x 6	**3.32**
$(B - K - B)_{min}$	87.21(17)
$(B - K - B)_{max}$	92.79(17)

Table S4. Interatomic distances in $(CH_3)_4NY(BH_4)_4$ crystal; results from periodic DFT calculations and PXD Rietveld refinement.

$(CH_3)_4NY(BH_4)_4$	**DFT**	**PXD**
$(B - H)_{min}$	1.206	1.15(6)
$(B - H)_{max}$	1.251	1.15(6)
$(H - B - H)_{min}$	105.68	109(5)
$(H - B - H)_{max}$	112.54	109(5)
$(Y - H)_{min}$	2.281	2.29(3)
$(Y - H)_{max}$	2.313	2.318(9)
$(Y - H)_{averag.}$ x 12	**2.296**	**2.296**
$(Y - B)_{min}$	2.447	2.394(11)

$(Y - B)_{max}$	2.471	2.430(9)
$(Y - B)_{averag.}$ x 4	**2.454**	**2.407**
$(B - Y - B)_{min}$	107.46	107.5(6)
$(B - Y - B)_{max}$	111.19	115.5(4)
$(N - B)_{min}$	4.268	4.400(19)
$(N - B)_{max}$	5.028	5.043(12)
$(N - B)_{averag.}$ x 9	**4.743**	**4.770**
$(N - Y)_{min}$	5.616	5.804(7)
$(N - Y)_{max}$	6.150	6.037(8)
$(N - Y)_{averag.}$ x 6	**5.920**	**5.904**

Table S5. Comparison of the ranges of bond lengths and angles in selected borohydrides. Units: V_m (molar volume) [Å^3], distances [Å], angles [^{O}].

	Quasi–binary borohydrides			Quasi–ternary Sc borohydrides			Quasi–ternary Y borohydrides	
Value or range	KBH_4 Fm–3m Error! Bookmark not defined.	$(CH_3)_4NBH_4$ P4/nmm Error! Bookmark not defined.	LT–$Y(BH_4)_3$ Pa–3 Error! Bookmark not defined.	$LiSc(BH_4)_4$ P–42c Error! Bookmark not defined.	$NaSc(BH_4)_4$ Cmcm Error! Bookmark not defined.	$KSc(BH_4)_4$ Pnma Error! Bookmark not defined.	$KY(BH_4)_4$ Cmcm	$(CH_3)_4NY(BH_4)_4$ Pnma
V_m	76.1	177.1	159.8	222.2	218.7	234.1	256.4	386.6
Wt. % H*	7.5	4.5	9.1	14.5	12.7	11.2	8.6	7.2
M^I–H**	2.877(11)	3.90(5)–5.91(4)	—	1.98(8)–2.5(1)	2.33(1)–3.34(1)	2.58(7)–3.69(12)	2.60(4)–3.37(3)	3.899(8)–5.957(12)
M^I–B**	3.3640(6)	4.533(6)–5.246(8)	—	2.54(1)	2.94(1)–3.22(1)	3.51(4)–3.95(2)	3.259(10)–3.354(7)	4.400(19)–5.043(12)
B–M^I–B**	90	70.25(17)–121.57(19)	—	73.0(3)–101.257(15)	87.76(2)–92.24(2)	57.3(4)–111.8(4)	87.21(17)–92.79(17)	49.09(16)–122.4(3)
M^{III}–H	—	—	2.229(8)–2.334(7)	1.92(5)–2.55(8)	2.15(2)–2.17(2)	2.0(1)–2.4(1)	2.20(3)–2.41(4)	2.29(3)–2.318(9)
M^{III}–B	—	—	1.176(10)–1.235(9)	2.28(1)	2.27(1)–2.50(1)	2.27(2)–2.38(3)	2.362(9)–2.448(10)	2.394(11)–2.430(9)
B–M^{III}–B	—	—	78.6(2)–105.0(2)	95.5(14)–114.9(5)	96.5(5)–125.4(5)	108.9(5)–110.6(6)	108.44(16)–112.3(4)	107.5(6)– 115.5(4)

(*) wt. % of H in pure compound; (**) M^I corresponds to N atom for $(CH_3)_4N$ salts.

Infrared spectra of $Y(BH_4)_3/MBH_4$ composites.

The vibrational spectra of $KY(BH_4)_4$ an $(CH_3)_4NY(BH_4)_4$ confirm structural aspects described earlier. The B–H stretching (ν_{BH} = 2100–2600 cm^{-1}) and H–B–H deformation (δ_{HBH} = 1050–1400 cm^{-1}) absorption bands are very similar to those for analogous scandium compounds, $MSc(BH_4)_4$, and characteristic for tridentate BH_4^- group.[1] The ν_{BH} bands are split into two groups, around 2475 cm^{-1} and 2150–2300 cm^{-1}, which has been assigned to stretching of the terminal hydrogen–B and bridging hydrogen–B bonds, respectively. The most important IR bands of these two compounds are summarised and compared with those for Sc borohydrides in *Tab S3*.

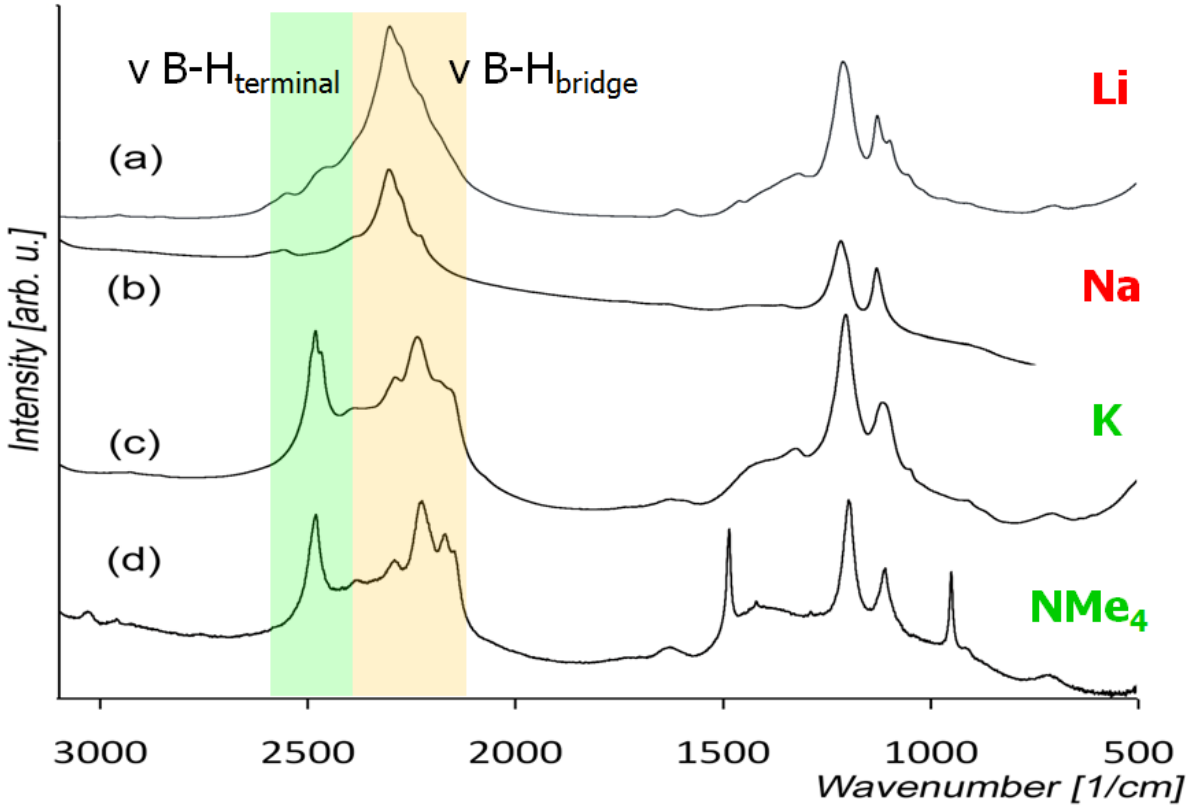

Figure S6. Infrared spectra of $Y(BH_4)_3$ + MBH_4 composites. MBH_4 = (a) $LiBH_4$, (b) $NaBH_4$, (c) KBH_4, (d) $(CH_3)_4NBH_4$.

Table S7. The most important infrared absorption bands in the as-synthesised Y compounds compared with Sc analogues. vs – very strong, s – strong, w – weak, vw – very weak, sh – shoulder.

$LiSc(BH_4)_4$ P-42c	$NaSc(BH_4)_4$ Cmcm	$KY(BH_4)_4$ Cmcm	$KSc(BH_4)_4$ Pnma	$(CH_3)_4NY(BH_4)_4$ Pnma	Assignment
-	-	-	-	3032 w 2964 vw	C-H stretching
2468	2486 2461	2482 vs 2468 sh	2506 sh 2485	2480 vs	$B\text{-}H_{terminal}$ stretching

2259 2240 2199 2121 w	2240 2160	2290 2236 vs 2183 sh 2156 sh	2288 2223	2291 2227 vs 2170 2148 sh	$B\text{-}H_{bridge}$ stretching
-	-	-	-	1484 s 1418 vw	H-C-H deformations
1325	1340	1324	1337 w	1288 vw	$H\text{-}B\text{-}H_{terminal}$ deformations
1194 vs	1189 vs	1203 vs	1188 vs	1196 vs	$H\text{-}B\text{-}H_{bridge}$ deformations
1113 1071 w	1105	1114 s 1050 sh	1121 1109 sh 1091 sh	1109 s	H-B-H deformations
-	-	-	-	949 s 912 vw	NC_4 breathing

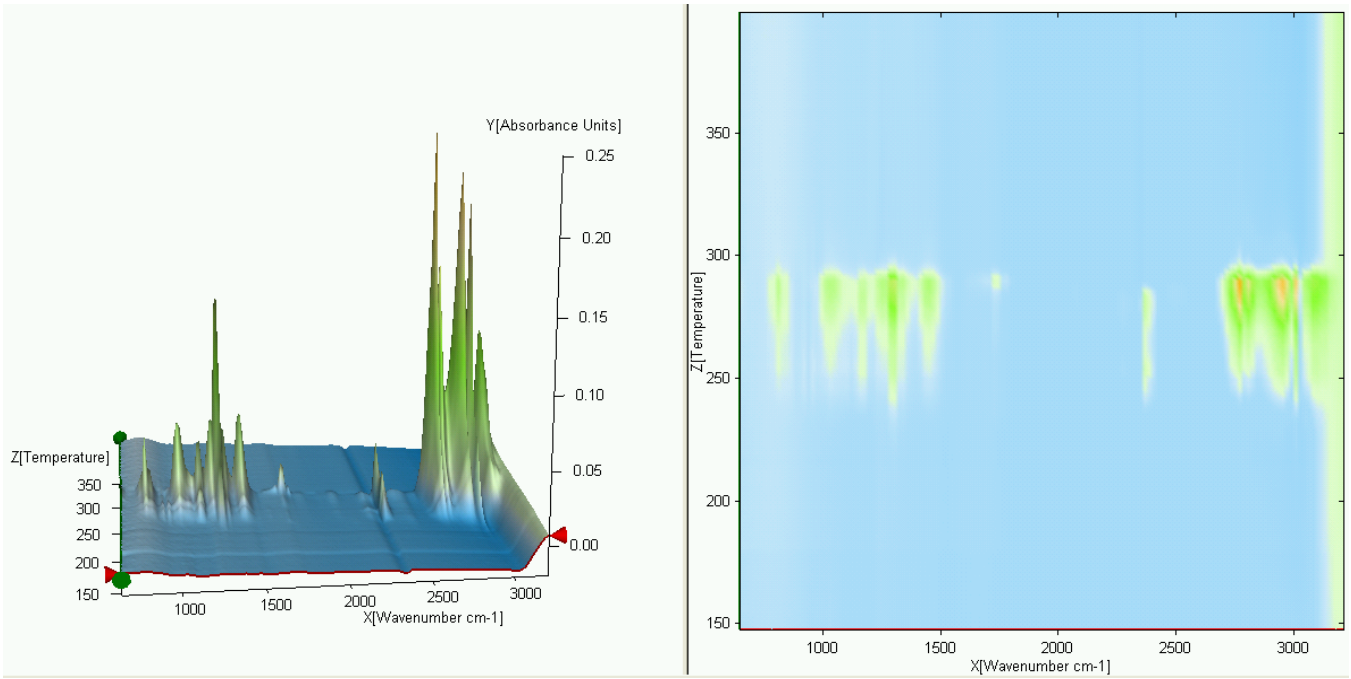

Figure S8. Temperature-resolved FTIR spectrum of the gases evolved during the thermal decomposition of $(CH_3)_4NY(BH_4)_4$ (5 K/min).

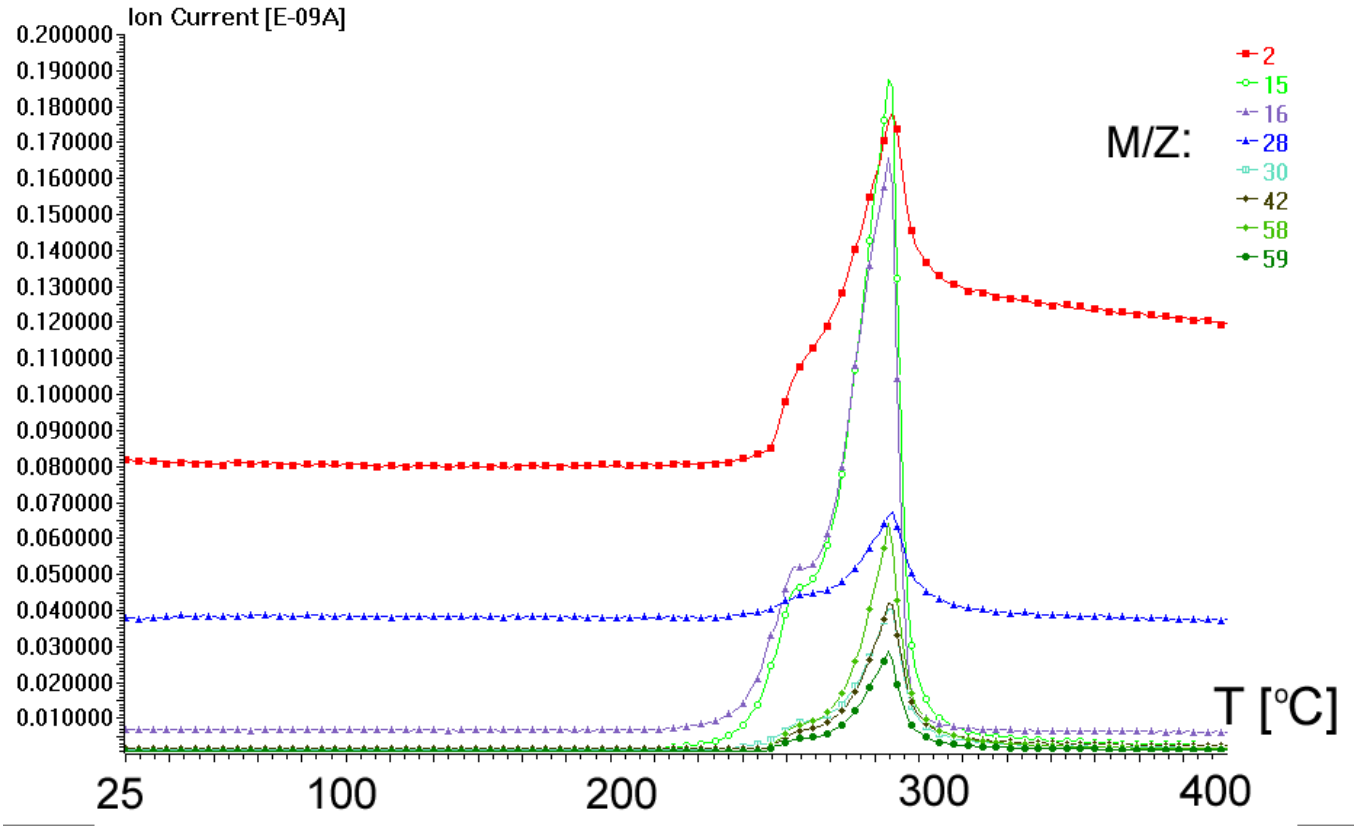

Figure S9. MS of the gases evolved in the thermal decomposition of $(CH_3)_4NY(BH_4)_4$ (5 K/min). Only the most important M/Z are shown.

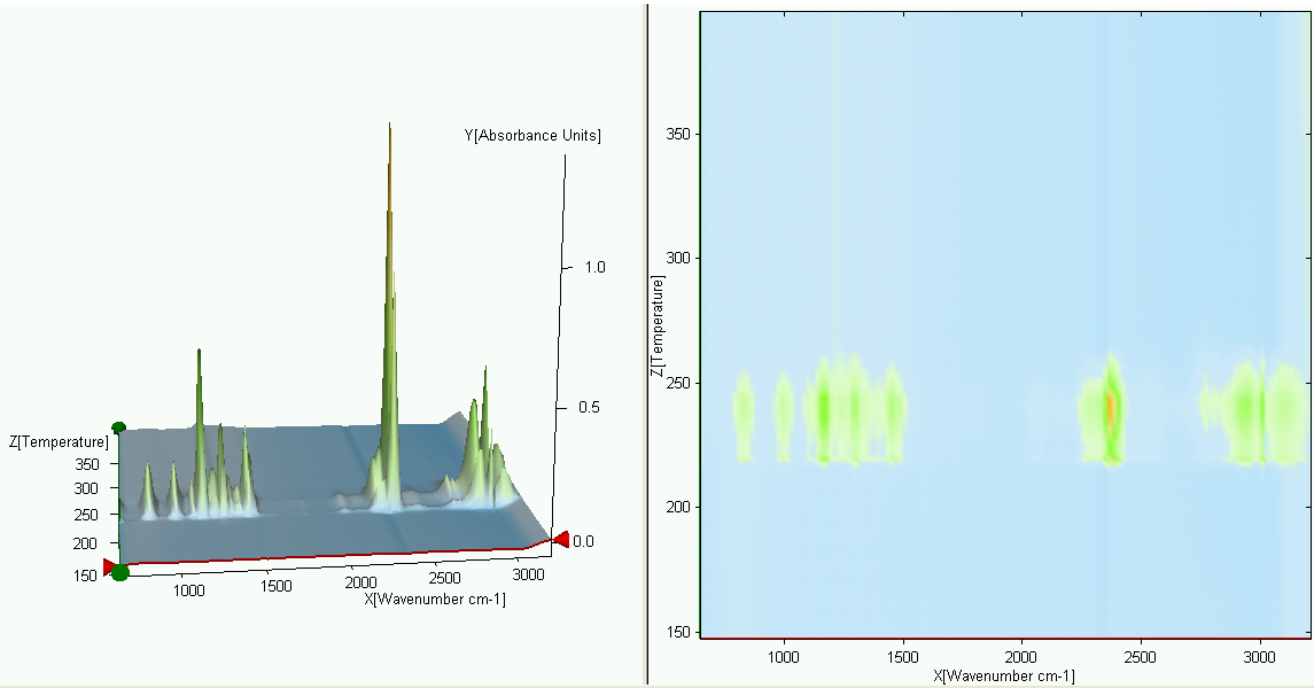

Figure S10. Temperature-resolved FTIR spectrum of the gases evolved during the thermal decomposition of $(CH_3)_4NBH_4$ (5 K/min).

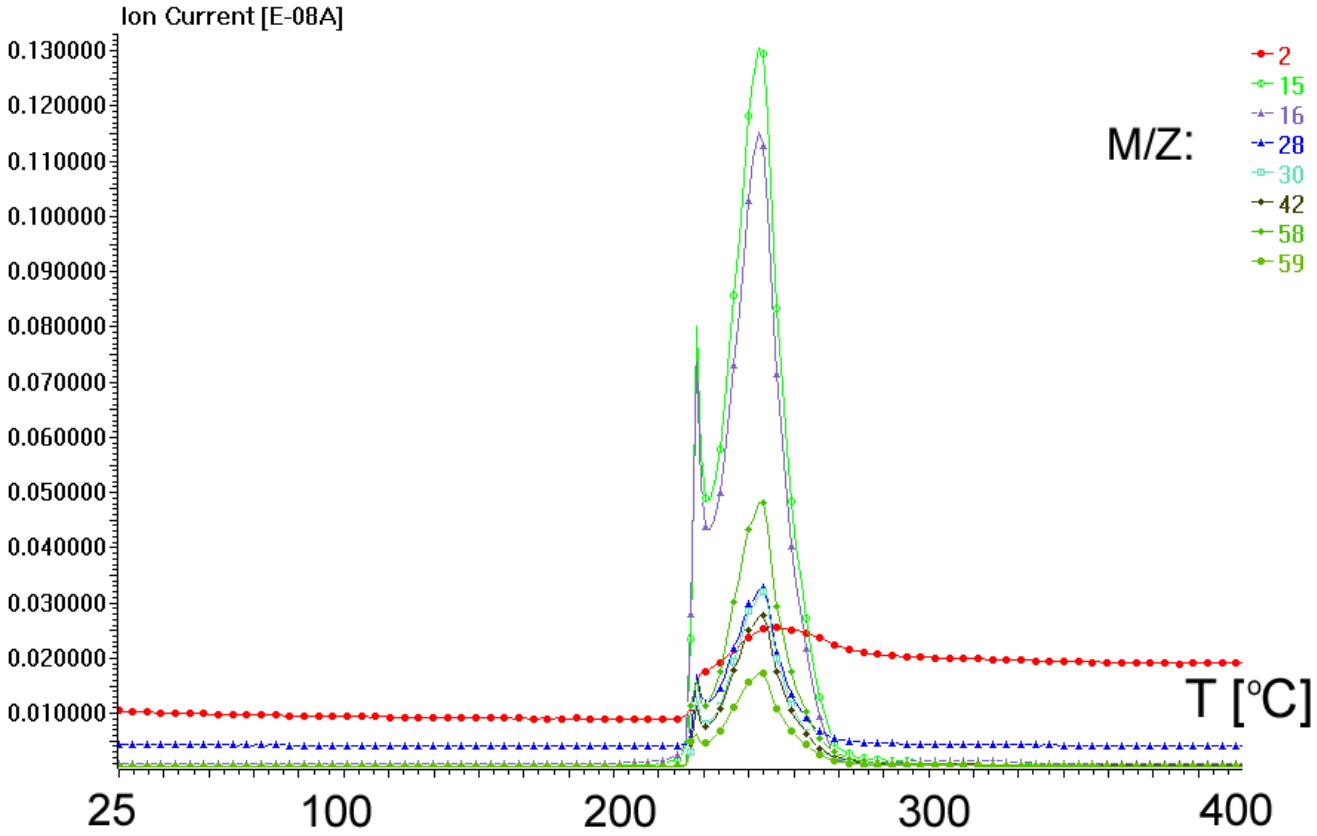

Figure S11. MS of the gases evolved in the thermal decomposition of $(CH_3)_4NBH_4$ (5 K/min). Only the most important M/Z are shown.

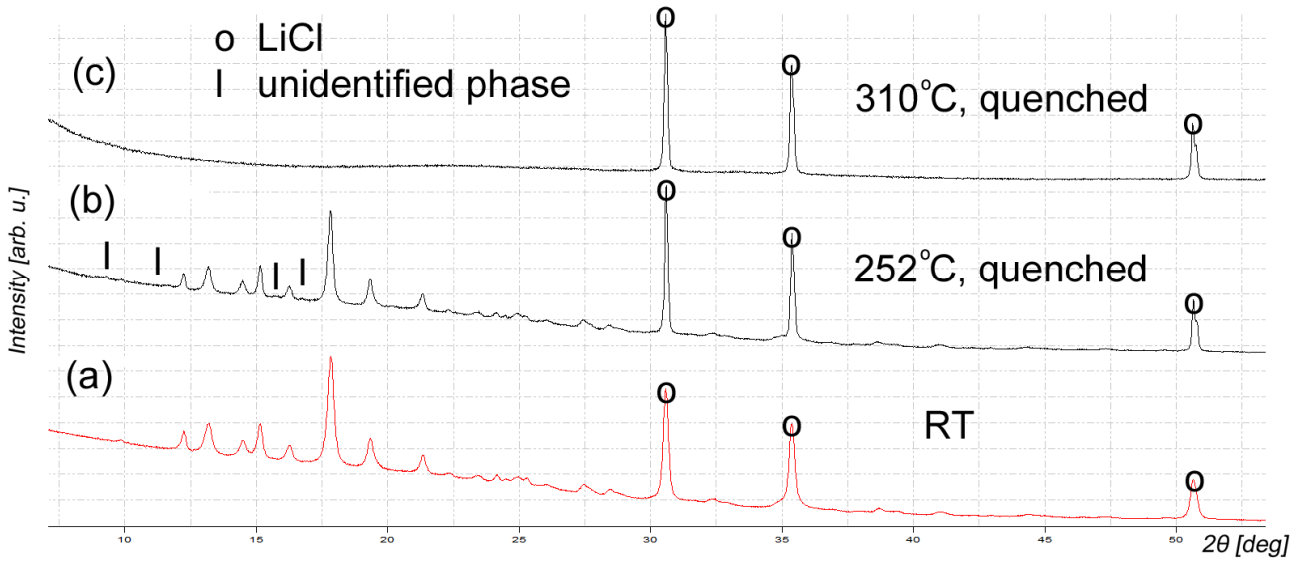

Figure S12. PXD of the thermal decomposition products of $(CH_3)_4NY(BH_4)_4$. The unmarked reflexes come from $(CH_3)_4NY(BH_4)_4$.

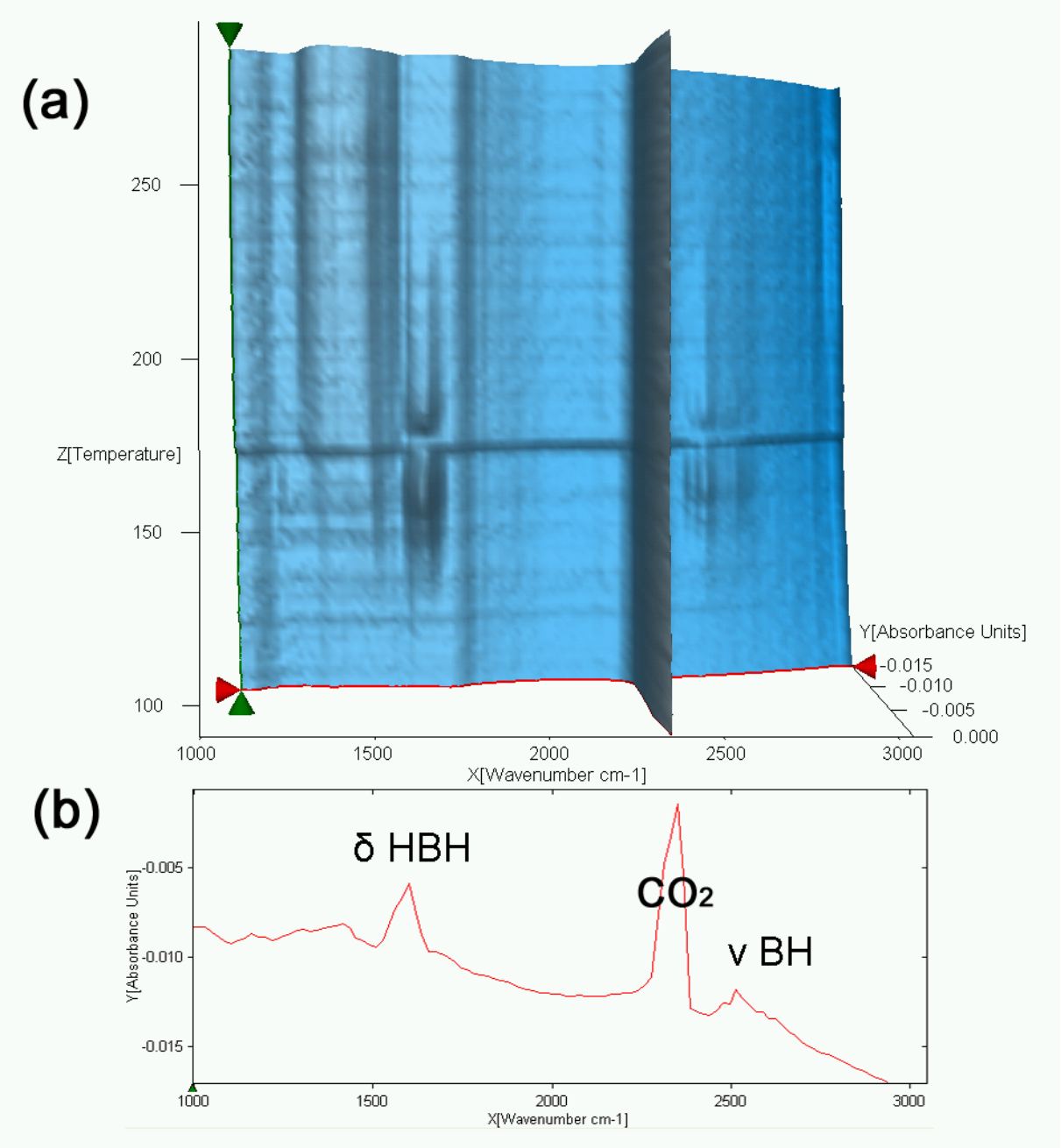

Figure S13. (a) Temperature-resolved FTIR spectrum of the gases evolved during the thermal decomposition of $KY(BH_4)_4$, (b) the single spectrum at a maximum B_xH_y emission (T = ca. 160 ^{O}C).CO_2 present in the atmosphere of the spectrometer (but not inside the gas cell) has not been completely compensated.

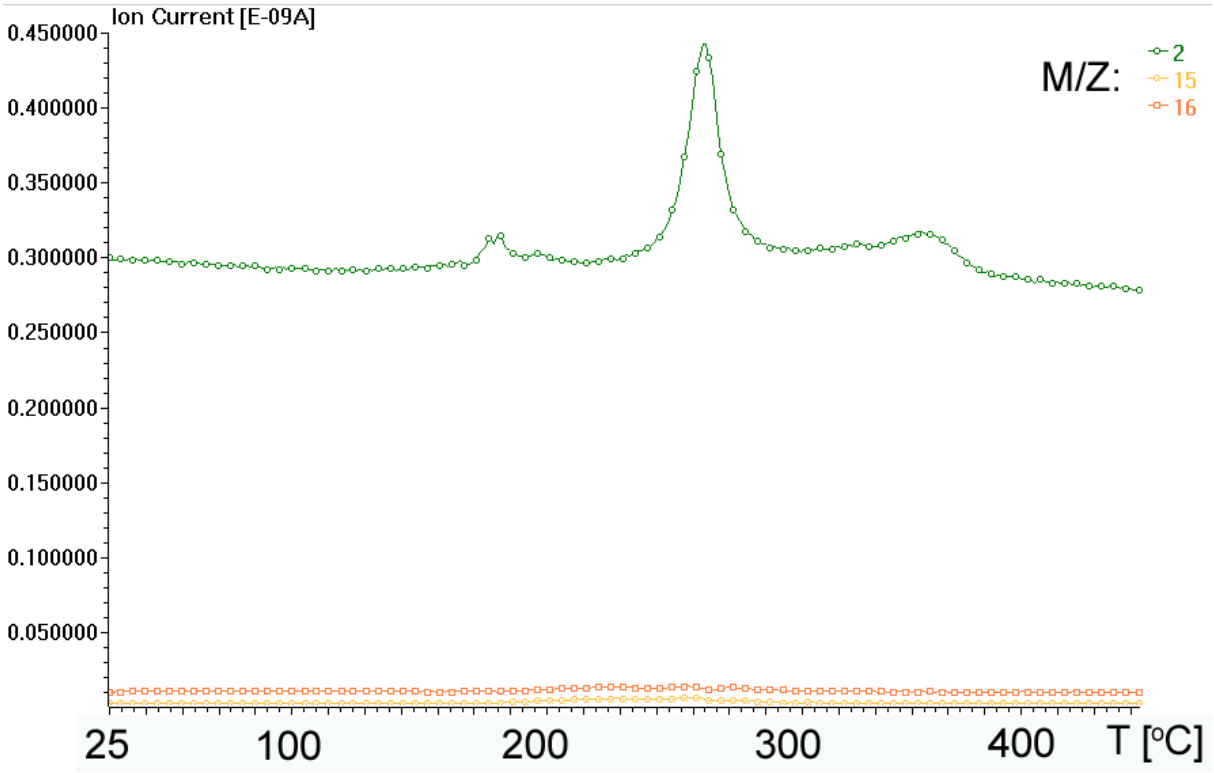

Figure S14. MS of the gases evolved in the thermal decomposition of K $Y(BH_4)_4$ (5 K/min). Only the most important M/Z are shown.

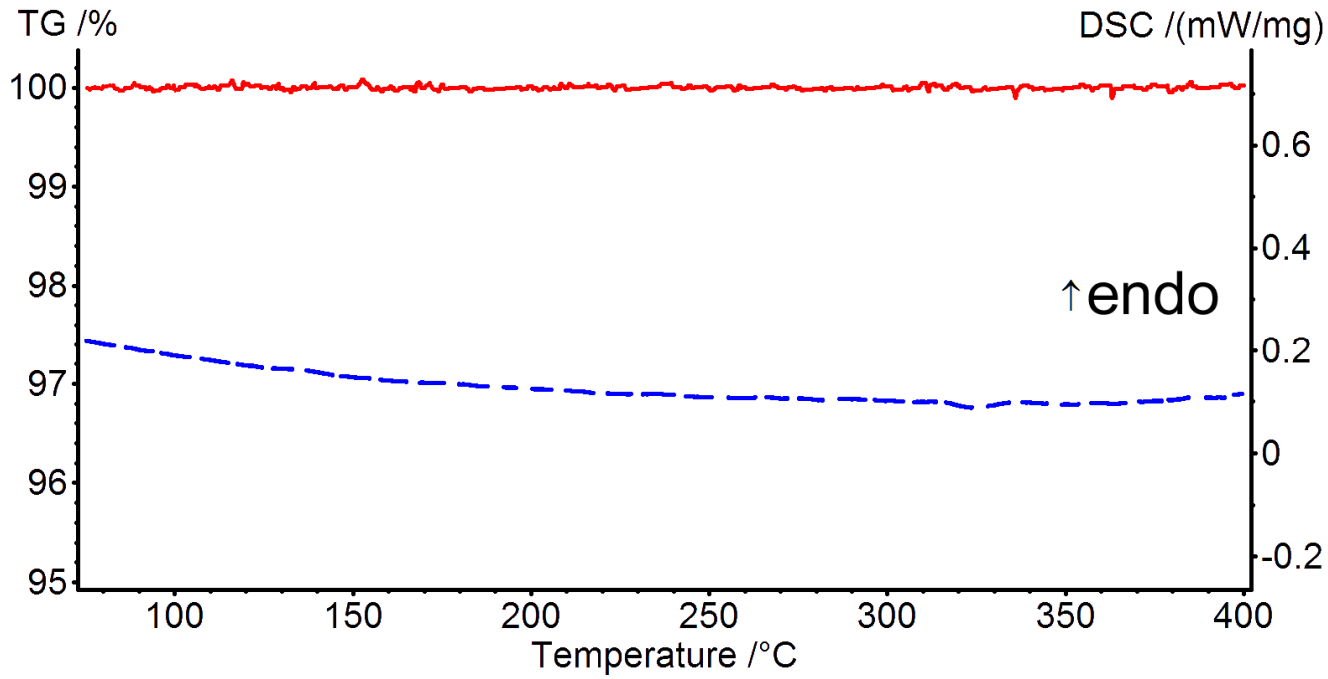

Figure S15. TGA (red, full line) and DSC (blue, dashed line) curves of KBH_4 milled for 1 h (5 K/min).

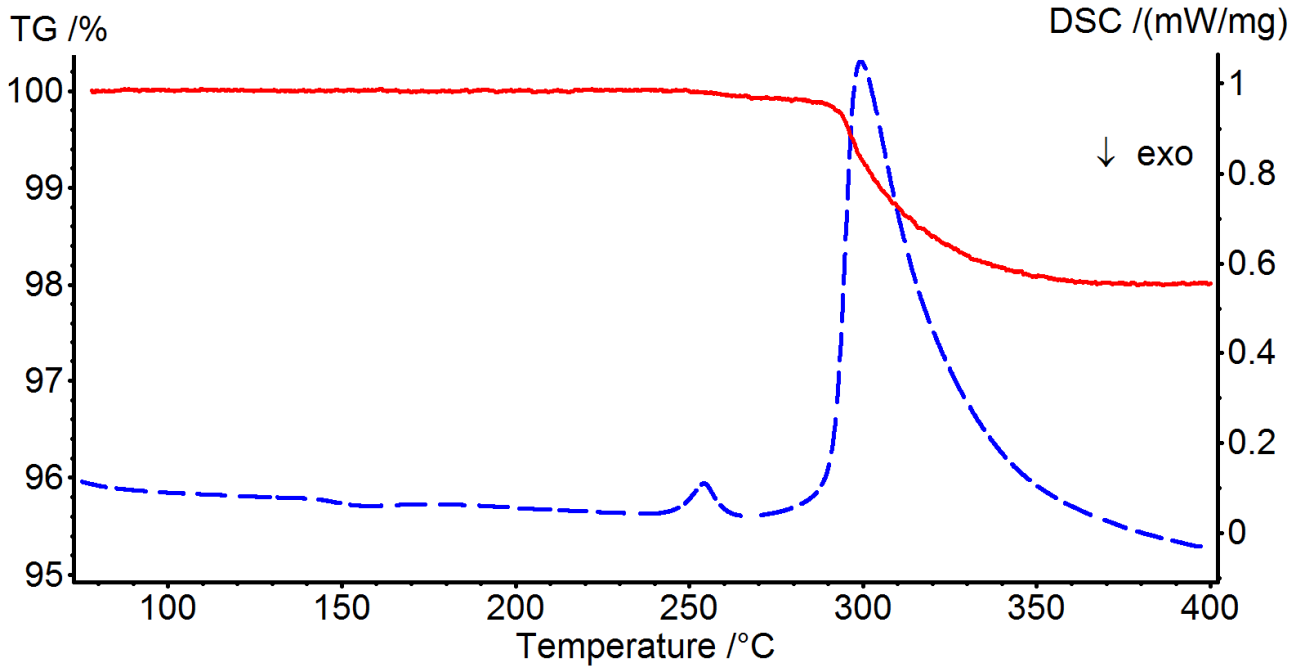

Figure S16. TGA (red, full line) and DSC (blue, dashed line) curves of $3KBH_4 + YCl_3$ milled for 1 h (5 K/min).

Figure S17. FTIR spectra of $KY(BH_4)_4$ thermal decomposition products: (a) as synthesised, (b) heated to 210 ^{O}C and cooled to RT, (c) heated to 295 ^{O}C and cooled to RT, (d) heated to 410 ^{O}C and cooled to RT, (e) KBH_4, (f) YH_x.[2]

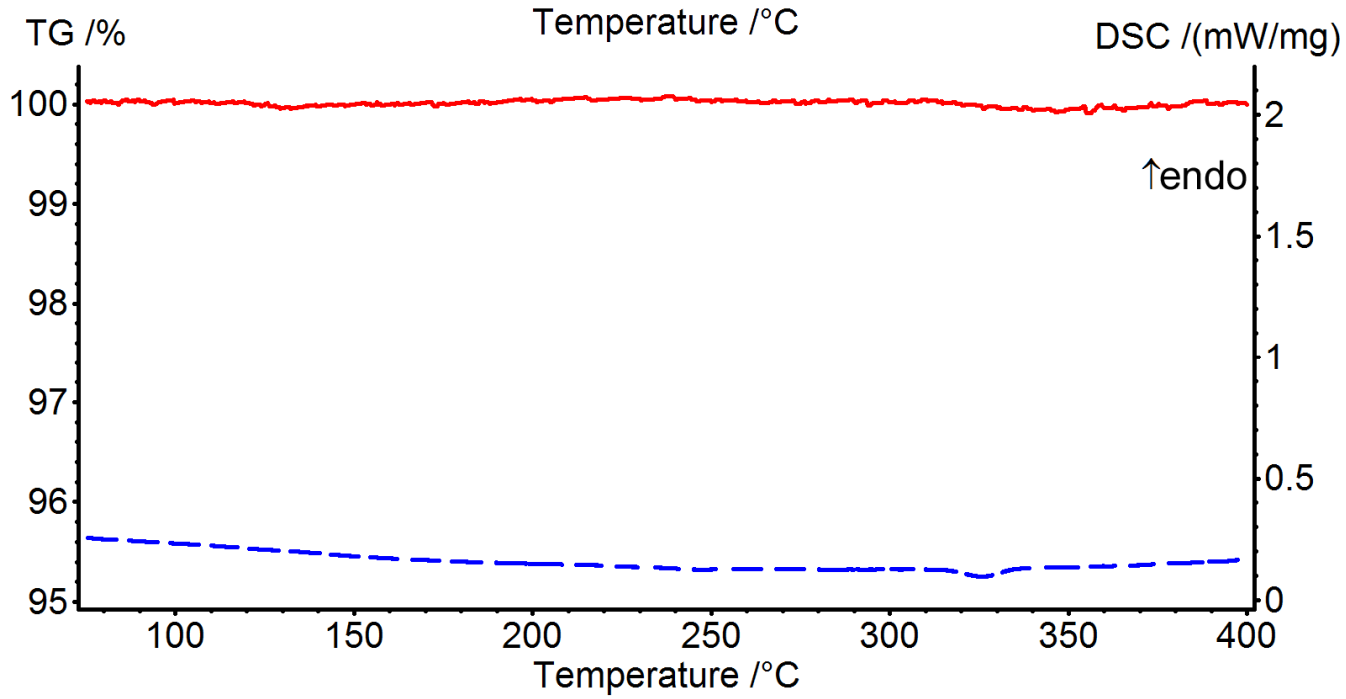

Figure S18. TGA (red, full line) and DSC (blue, dashed line) curves of $NaBH_4$ milled for 1 h (5 K/min).

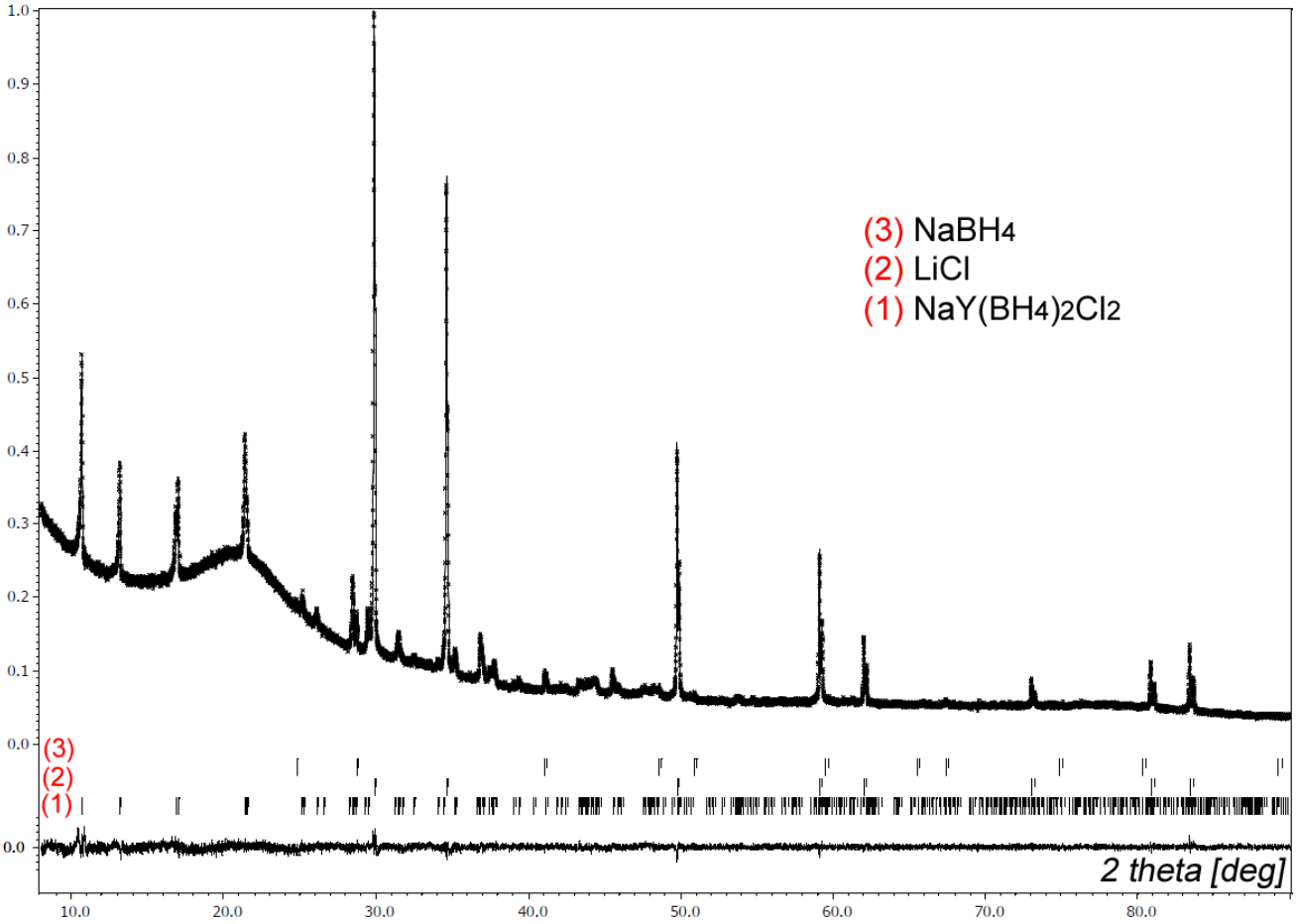

Figure S19. Rietveld plot of $Y(BH_4)_3$ + $NaBH_4$ + 3 LiCl composite measured at 171 ^{O}C. BH_4^- sites in $NaY(BH_4)_2Cl_2$ are partially occupied by Cl^-, leading to composition: $NaYCl_{2.18}(BH_4)_{1.82}$.

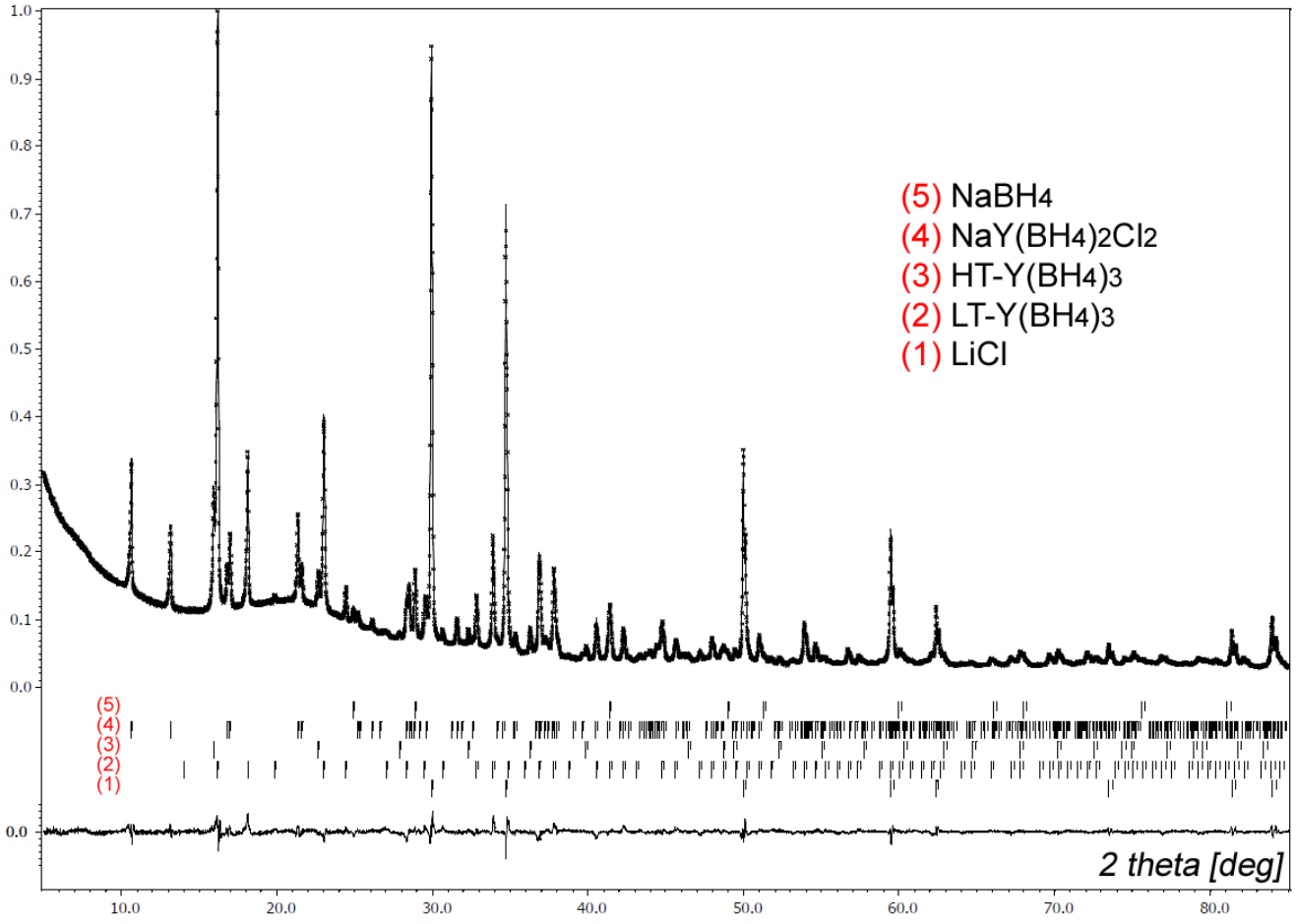

Figure S20. Rietveld plot of $Y(BH_4)_3$ + $NaBH_4$ + 3 LiCl composite heated to 200 ^{O}C (5 K/min) and rapidly quenched (50 K/min); PXD measured at RT. BH_4^- sites in $NaY(BH_4)_2Cl_2$ are partially occupied by Cl^-, leading to composition: $NaYCl_{2.09}(BH_4)_{1.91}$. Please, note the minor Cl substitution degree, which is probably due to shorter exposition to high temperature than in case of the sample measured at 171 ^{O}C.

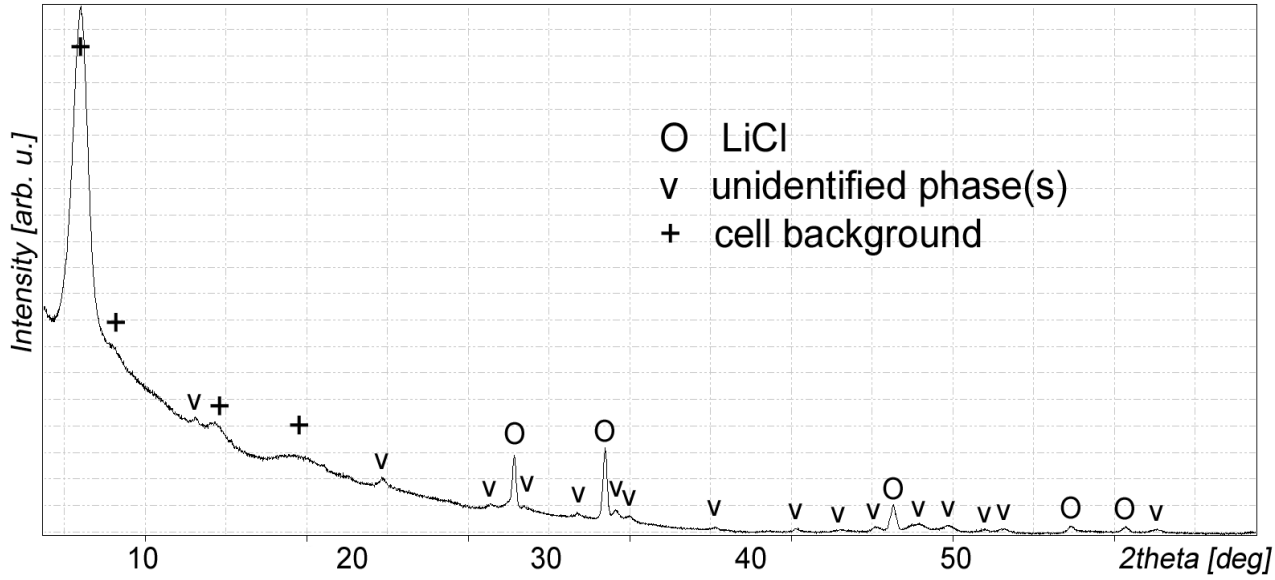

Figure S21. PXD pattern of $Y(BH_4)_3$ + $NaBH_4$ + 3 LiCl composite measured at 400 ^{O}C. The reflexes originating from the heating cell have been marked.

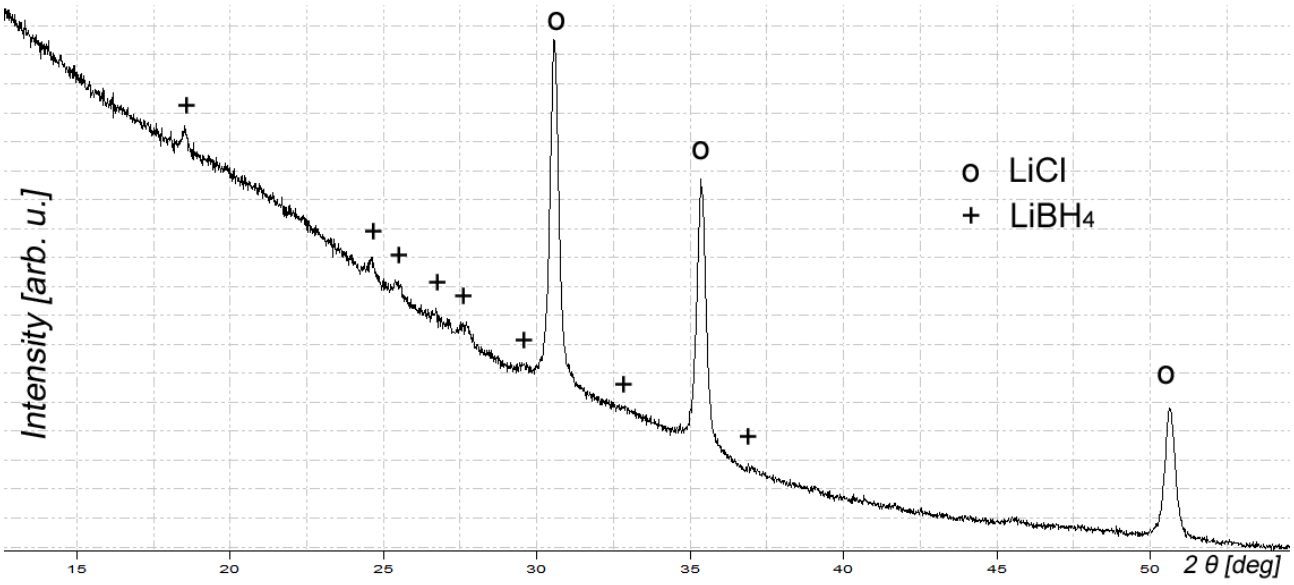

Figure S22. PXD pattern of $Y(BH_4)_3$ + $LiBH_4$ + 3 LiCl composite heated to 210 ^{O}C and quickly quenched to room temperature. Measured at ambient conditions.

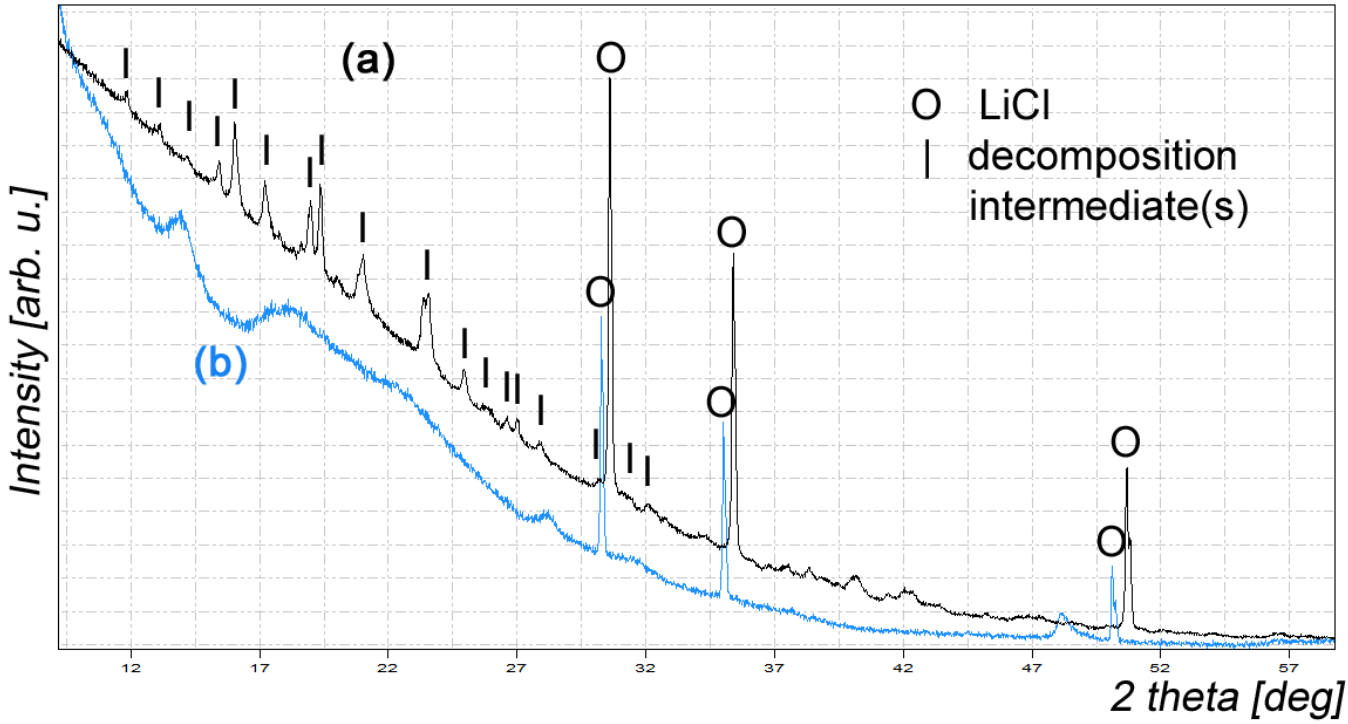

Figure S23. PXD pattern of $KY(BH_4)_3$ + 3 LiCl: (a) sample heated to 210 ^{O}C and quickly quenched to room temperature (black, top curve), measured for 17 h at room temperature; (b) measured at 200 ^{O}C for 5.5 h. In (b) only the reflexes from the temperature cell (not marked) and those of LiCl are observed, while in (a)the reflexes from intermediate(s) appear. The intermediate phase has been detected in the samples heated to 190 – 210 ^{O}C and quenched rapidly to room temperature.

[1] T. J. Marks, and J. R. Kolb, *Vhem. Rev.*, **77** (1977) 263.

[2] FTIR spectrum of YH_x was kindly provided by R. V. Genova, M.Sc., and K. J. Fijałkowski, M.Sc..